Thermal Release of Inert Gases from a (100) Tungsten Surface

E. V. Kornelsen and M. K. Sinha

Citation: Journal of Applied Physics **39**, 4546 (1968); doi: 10.1063/1.1655799
View online: http://dx.doi.org/10.1063/1.1655799
View Table of Contents: http://scitation.aip.org/content/aip/journal/jap/39/10?ver=pdfcov
Published by the AIP Publishing

on smooth insulating substrates but not on rougher oxides. (7) Conductivity modulation was observed in Cs layers adsorbed on ferroelectric $BaTiO_3$ both below and above the Curie temperature. (8) Photoemission measurements show that the conductivity modulation is primarily due to a difference in the number of electrons in the film for the two polarizations. (9) The noise in the adsorbed Cs film is proportional to the square root of the resistance but is about 15 times as great as the theoretical thermal noise. (10) The equilibrium film probably corresponds to one close-packed monolayer. (11) The conduction in the equilibrium film is close to that predicted by surface-scattering reduction of the bulk conductivity.

ACKNOWLEDGMENTS

The author wishes to express his sincere appreciation for the guidance and encouragement of Professor R. S. Muller during the course of the project. The author would also like to thank Dr. A. M. Goodman of RCA Laboratories for suggesting the project and Bell Telephone Laboratories, Dow Chemical Co., DuPont, Philco-Ford Microelectronics Division, and RCA Laboratories for supplying experimental materials.

JOURNAL OF APPLIED PHYSICS VOLUME 39, NUMBER 10 SEPTEMBER 1968

Thermal Release of Inert Gases from a (100) Tungsten Surface

E. V. KORNELSEN AND M. K. SINHA*

Radio and Electrical Engineering Division, National Research Council, Ottawa, Canada

(Received 8 March 1968)

A clean (100) tungsten surface has been bombarded with beams of 40 eV to 5 keV ions of Ne, Ar, Kr, and Xe. Gas desorption rates, measured as the crystal was subsequently heated at 40°K/sec, show a number of fairly clearly defined peaks between 400° and 2200°K. The characteristics of these peaks with varying ion energy, mass, and direction of incidence suggest the following interpretation: (a) All peaks below 1650°K (4 for Ne, 5 for Ar, Kr, and Xe) are the result of desorption via a single activated step from sites within, at most, 10 Å of the crystal surface, and (b) the single peak above 1700°K is the result of isotropic diffusion of more deeply penetrating ions with an activation energy 104 kcal/mole, the same for all four gases.

INTRODUCTION

An inert gas ion incident upon a solid surface with sufficient kinetic energy may enter the solid and come to rest there. The probability that such an entrapment will occur at room temperature rises from near zero at ~10 eV impact energy to near unity at 10^4 eV. Throughout this interval, the collisions between the ion and the atoms of the solid are quasielastic, and the depth of penetration is small enough that the surface plays a significant role in the entrapment. Some information concerning the binding energies of the trapped particles can be obtained by raising the temperature of the solid and observing the rate of evolution of the trapped gas. The release-rate spectrum or 'desorption spectrum' for a given temperature profile can in principle by analyzed, using the first-order desorption equation,[1,2] to yield the entire binding-energy spectrum of the trapped particles.[3] In practice, the inherently limited resolving power (about 12) makes such a deconvolution difficult even for the best obtainable data, so that only the peaks in the energy spectrum, corresponding to the desorption-rate maxima, can be easily identified. It should also be kept in mind that the gas release may pertain to a quite different trapping configuration than that in which the ion came to rest at the bombardment temperature, since intermediate stages of annealing may occur as the solid is heated.

In experiments reported to date, analysis has been made even more difficult by very complex conditions at the trapping surface. Earlier experiments on metals[4–8] involved polycrystalline targets and poorly defined directions of ion incidence. The possible influence of grain boundaries, different exposed crystal planes, and varying angles of incidence could therefore not be determined. Some experiments on ionic single crystals have been reported[9] but these probably had surfaces contaminated by adsorption.

Thermal release of inert gases from copper monocrystals following higher-energy bombardment ($\geq$20 keV) has recently been reported.[10,11] In these cases, the penetration depths were large enough that the

* Present address: Physics Dept., North Dakota State University, Fargo, N.D.

[1] P. A. Redhead, Vacuum **12,** 203 (1962).
[2] G. Carter, Vacuum **12,** 245 (1962).
[3] G. Farrell and G. Carter, Vacuum **17,** 15 (1967).
[4] R. B. Burtt, J. S. Colligon, and J. H. Leck, Brit. J. Appl. Phys. **12,** 396 (1961).
[5] E. V. Kornelsen, Can. J. Phys. **42,** 364 (1964).
[6] K. Erents and G. Carter, Vacuum **16,** 523 (1966).
[7] K. Erents and G. Carter, Vacuum **17,** 215 (1967).
[8] K. Erents, R. P. W. Lawson, and G. Carter, J. Vac. Sci. Technol. **4,** 252 (1967).
[9] R. Kelly and H. J. Matzke, J. Nucl. Mater. **17,** 179 (1965).
[10] B. Perovic and T. Jokic, Phys. Letters **20,** 485 (1966).
[11] T. Jokic and B. Perovic, Can. J. Phys. **46,** 635 (1968).

TABLE I. Gauge voltages and sensitivities (G).

	V_{f-c}[a] (V)	V_{g-c}[a] (V)	G at $I^-=8$ mA (A/Torr)
Ne	20	100	0.0333
Ar	7	52	0.1100
Kr	7	52	0.1505
Xe	7	52	0.252

[a] Voltages relative to ion collector.

influence of the contaminated surface was probably not significant. The effect of the crystallographic direction of ion incidence could be clearly seen in the gas release spectra.

To eliminate the ambiguities resulting from polycrystalline targets and unknown angles of incidence, we have studied the entrapment of inert gas ions arriving in a collimated beam at carefully prepared low-index crystal faces of tungsten in ultrahigh vacuum. Ion energies ranged from 40 eV to 5 keV and the dose (number incident) from 3×10^{12}–1.5×10^{13} ions/cm^2. The gas-release rate was measured as the crystal temperature was subsequently raised at 40°K/sec from 300° to 2400°K. Preliminary reports showing the variation of release spectra for identical bombardments of three different faces have already appeared in a letter[12] and in the proceedings of a recent conference.[13] The present paper gives details of the experimental technique and of the influence of ion energy and mass on the release spectra from a (100) tungsten surface. A second paper[14] giving comparable data for (110) and (211) surfaces is in preparation to complete the detailed presentation. A short paper describing details of the apparatus is also planned.[15]

APPARATUS

The experiments were performed in a glass-envelope ultrahigh-vacuum system, of a type described previously.[16] The system is shown schematically in Fig. 1. The components and their arrangement are basically the same as described in earlier work on polycrystalline tungsten,[5] (hereafter referred to as paper I). Some minor modifications of technique are mentioned in the description of the experimental method.

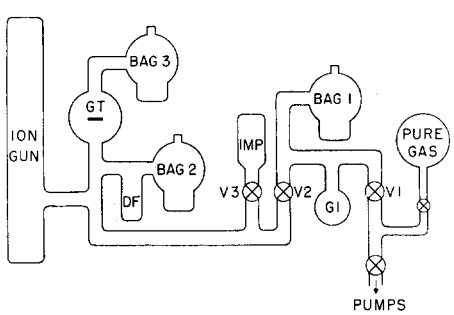

FIG. 1. Schematic diagram of the vacuum system. IMP is a cold-cathode inverted magnetron ion pump.[16]

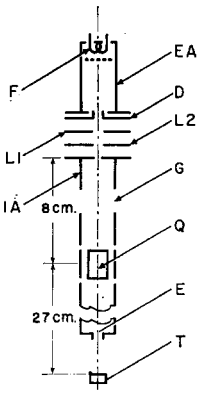

FIG. 2. Schematic diagram of the ion gun: F: 0.0125-cm-diam thoria-coated filament, EA: electron anode, D: draw-out plate, L_1, L_2: aperture lenses, IA: ion accelerator, G: high-voltage accelerating gap (cylinder lens), Q: quadrant deflectors, also used as an Einzel lens, E: 0.5-cm-diam exit aperture, and T: target crystal.

The gauge marked BAG 1 monitored the quantity of gas admitted through valve V1 to perform the ion bombardment. Gauge BAG 2 and the desorption filament DF were operated only during the determination of chemisorbable gas partial pressures. They were turned off completely during the bombardment-desorption experiments. The gauge used to detect the gas release (BAG 3) was separated from the crystal by an evaporated titanium "getter trap" GT. Most of the H_2 and N_2 released from the crystal during the desorption cycle was thus prevented from reaching BAG 3 and interfering with the desired inert gas pressure. The measured H_2 pressure ratio across GT

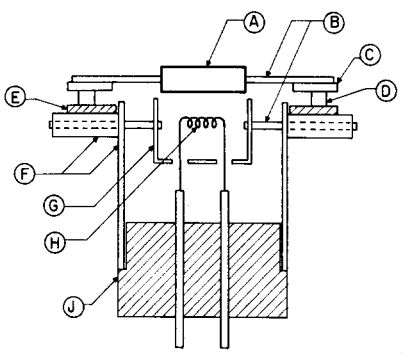

FIG. 3. Schematic of the crystal mount and bombardment heater: A: target crystal, B: tungsten pins, C: molybdenum mounting ring, D: platinum leveling feet, E: alumina insulating ring, F: molybdenum bombarding structure, G: tungsten cup, H: tungsten bombarding filament ($L=2$ cm, $D=0.0125$ cm), and J: alumina filament mounting block.

[12] E. V. Kornelsen and M. K. Sinha, Appl. Phys. Letters **9**, 112 (1966).
[13] E. V. Kornelsen and M. K. Sinha, Can. J. Phys. **46**, 613 (1968).
[14] E. V. Kornelsen and M. K. Sinha (unpublished).
[15] E. V. Kornelsen (unpublished).
[16] P. A. Redhead, E. V. Kornelsen, and J. P. Hobson, Can. J. Phys. **40**, 1814 (1962).

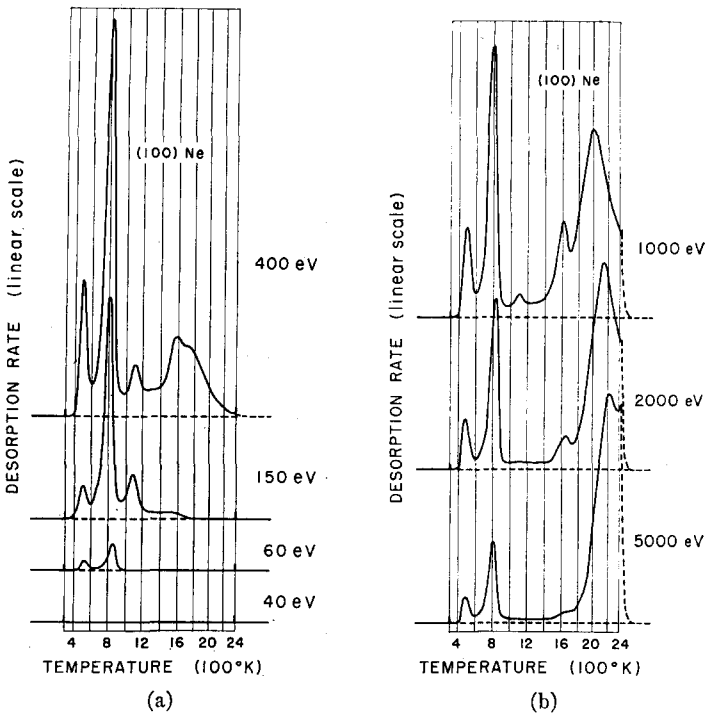

FIG. 4. (a) Desorption spectra for low-energy Ne^+ ions. (b) Desorption spectra for higher-energy Ne^+ ions.

was typically 100. As in I, BAG 3 was operated at 8 mA electron emission with voltages reduced to limit its ionic pumping speed to 2×10^{-3} liter/sec. Table I summarizes the operating potentials and the corresponding gauge sensitivities. The latter were obtained by comparison, at $\sim10^{-7}$ Torr, with BAG 1 which was in turn calibrated against a McLeod gauge at $\sim10^{-3}$ Torr. The absolute sensitivities have uncertainties of $\pm5\%$.

The ion gun, which will be described in a separate paper,[15] is shown schematically in Fig. 2. The gas, at a pressure 10^{-7}–10^{-5} Torr, was ionized within the cylindrical electrode EA by 10 mA of electrons of energy below the threshold for double ionization. Other electrodes are identified in the figure caption. Retarding field analysis showed that 99% of the ions had energies within ±2 eV of the mean, independent of the beam energy. The ion beam currents were 1 to 3×10^{-2} A/Torr for pressures $\leq10^{-7}$ Torr, and reached maximum values $\sim2\times10^{-8}$ A at about 10^{-5} Torr.

The crystal mount and heating assembly, also to be described elsewhere,[15] are shown schematically in Fig. 3. The mount, consisting of the crystal A, the tungsten pins B, molybdenum ring C, and platinum feet D, was inserted as a unit through a side port in the gun envelope and set on the alumina insulating ring E. The angle of ion incidence could be selected (before evacuation) in 5 deg steps by rotation of the entire mount and heater about an axis in the crystal surface plane. In the present experiments, only normal incidence was used. During desorption, the bombarding current of electrons (1 kV) drawn from the tungsten filament H was varied automatically in a predetermined way to cause the crystal temperature to rise approximately linearly with time. The heating power cut off abruptly at the end of the cycle; the resulting initial rate of decrease of crystal temperature was ~300°K/sec.

The crystal temperature was measured with a recording ir pyrometer, which was calibrated above 1100°K against an optical pyrometer. Below 1100°K, emissivity corrections for the appropriate wavelength region were applied to obtain the temperature from the ir pyrometer signal using calibrations supplied by the manufacturer. The recording pyrometer indications vs time during heating were reproducible to ±10°K. The absolute accuracy of the temperature scale, affected by emissivity corrections, transmission through the envelope, and the accuracy of comparison of the optical pyrometer against a pyrometric standard, is estimated to be $\pm25°$ up to 1100°K, and $\pm40°$ at 2400°K.

The crystal, 7 mm in diameter and 2 mm thick, was cut from the same rod and by the same methods as those used earlier for studies of ion penetration depth.[17] The final surface was determined by x-ray back-reflection to be within 2 deg of (100). Both high- and low-energy electron diffraction studies gave the patterns expected of a (100) exposed face after the crystal had been heated to 2400°K in ultrahigh vacuum (uhv). (The diffraction experiments were

[17] E. V Kornelsen, F. Brown, J. A. Davies, B. Domeij, and G. R. Piercy, Phys. Rev. **136**, A849 (1964).

conducted in *separate* uhv systems.) The ion bombardment was limited to the central 5 mm of the crystal face, an area of 0.20 cm^2.

The portion of the system to the left of the valve V1 (Fig. 1) was baked for 16 h at 450°C during which a pressure of $\sim 10^{-6}$ Torr was indicated by an external sputter-ion pump. Following outgassing, and with the ion source fully operating, the total pressure was 8×10^{-11} Torr (equivalent N_2). Background partial pressures of chemisorbable gases were determined with the desorption filament DF and BAG 2. Hydrogen and nitrogen were identified, their partial pressures fluctuating between about 3×10^{-13} and 2×10^{-12} Torr. Desorption spectra obtained with BAG 2 during the heating of the crystal itself indicated that less than 0.01 monolayer of gas accumulated on its surface in 90 min (i.e., desorption peak heights following 90 min of adsorption did not exceed 0.01 of the maximum heights observed). The above conditions were attained about one week after bakeout.

The recording system consisted of an electrometer (Keithley model 410), a low-pass filter, a differentiator, and a chart recorder. The measured response time constant of the system was 0.4 sec, and the rms noise level on the differentiated signal was $1\text{–}2\times10^{-14}$ A/sec when the BAG 3 current was 2×10^{-11} A.

EXPERIMENTAL METHOD

The method used was the same, in principle, as that described in I (polycrystalline targets). For the present apparatus, each cycle of bombardment and desorption entailed the following steps:

(1) The crystal was heated at 40°K/sec to 2400°K to remove adsorbed gases. (The same heating schedule as used on desorption.)

(2) About 30 min later, when the crystal had cooled to <350°K, the inert gas was introduced through valve V1 (with V2 closed) and 4 or 5 min allowed for the chemisorbable impurities to be removed by the titanium getter G1.

(3) The ion gun potentials were applied, BAG 3 turned to 80 μA emission, V3 closed, and V2 opened to expand the gas into the gun and begin the bombardment. The increase in beam current over background upon opening V2 always exceeded a factor 300 once minor deflection and focusing adjustments had been made. The true ion current to the target was measured with an electrometer by connecting together the target and a surrounding hemisphere which collected the secondary electron current.

(4) When the desired total number of ions

$$[n_i=(1/e)\int_0^t i_x dl]$$

had struck the crystal, the gun was turned off and V3 opened to pump out the remaining inert gas.

(5) After a few minutes BAG 3 was switched back 8 mA emission, and V2 closed to restrict the reemission from BAG 1 to the inlet volume.

(6) When the pressure at the crystal had fallen sufficiently (usually to $<5\times10^{-10}$ Torr within 5 to

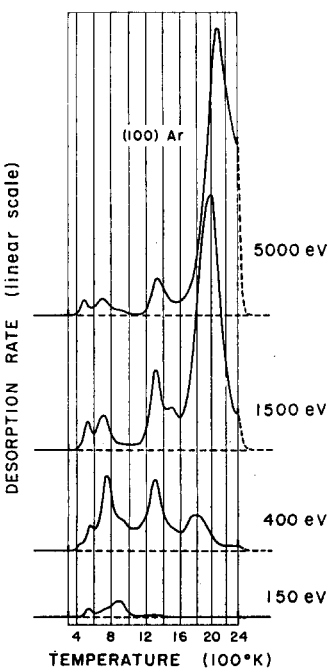

FIG. 5. Desorption spectra for Ar^+ ions of various energies.

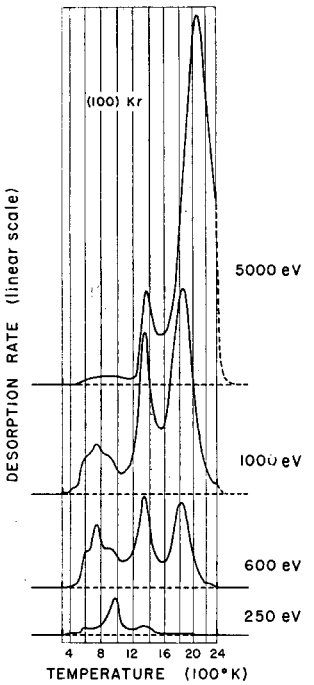

FIG. 6. Desorption spectra for Kr^+ ions of various energies.

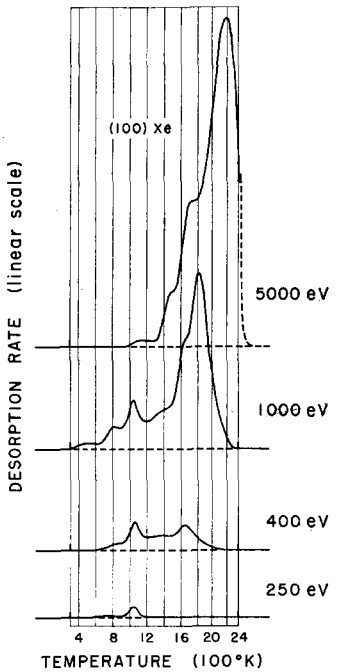

FIG. 7. Desorption spectra for Xe^+ ions of various energies.

10 min), V3 was closed to isolate the desorption volume (measured V=3.93 liter) from the pump.

(7) The desorption cycle was the initiated and the differentiated output of BAG 3 recorded.

(8) Finally V2 and V3 were opened and the desorbed gas pumped away.

The entire cycle required 60 to 90 min depending on the amount of gas introduced and the number of ions required. About 100 such cycles were performed during the experiments.

EXPERIMENTAL RESULTS

The basic results are presented as groups of desorption spectra in Figs. 4–7 (Ne, Ar, Kr, and Xe, respectively), with the energies of the bombarding ions indicated at the righthand side. Each spectrum consists of a plot of the rate of change of pressure on a linear scale against the crystal temperature in degrees Kelvin. The ordinate scales are the same for all spectra in any one figure and, although not indicated, can be converted to desorption rates (molecules/sec) using the known gauge sensitivity and system volume. The abscissa is a linear time scale on which the slightly nonlinear temperature scale has been constructed using calibration data. Vertical markers indicate the beginning and the end of the 50 sec desorption cycle. Many spectra were taken at energies intermediate to those shown in the figures. These did not reveal any qualitatively new features but occasionally showed particular peaks more clearly. The number, shape, and position of the observed peaks was independent of dose up to the values used in these experiments, and all peak amplitudes varied linearly with dose except for the case of neon, which will be discussed later.

Bombardment with low-energy Ne^+ ions gave the spectra shown in Fig. 4(a). In each case the dose was 1.5×10^{13} ions/cm^2. Ions of 40 eV energy gave no detectable gas desorption. (The detection limit for Ne on this electrometer scale was $\sim3\times10^{10}$ atoms/cm^2.) Although not included in all the figures, such a result was obtained for each of the gases when the ion energy was sufficiently low. This constitutes the most direct evidence that the observed desorption contains neither spurious effects nor experimental artifacts.

As the Ne^+ ion energy was increased to 60 eV, two peaks were observed to appear below 1000°K. Additional peaks appeared with further energy increase until, at 400 eV, five were clearly visible at temperatures near 500°, 800°, 1100°, 1600°, and 1800°K. The peak amplitudes increased rapidly with ion energy, whereas their positions on the temperature scale were independent of the ion energy to within experimental error. Increasing the ion energy still further [Fig. 4(b)], the amplitudes of the first four peaks decreased but their positions continued to be unchanged. The fifth peak increased in amplitude and also shifted to higher temperature, reaching 2200°K for 5 keV ions. The width of the fifth peak at half-amplitude is ~450°K, about a factor four wider than those at lower temperature. The single peak appearing above 1700°K is thus seen to behave in a qualitatively different way from all those at lower temperatures. To facilitate discussion, this peak will be called the "β-peak" and all those at lower temperatures "α-peaks".

The dotted lines on the spectra of Fig. 4(b) after the end of the heating period indicate the decrease in desorption rate during the rapid cooling of the crystal. The rate of fall was found to be limited by the time constant of the detecting system ($\tau=0.4$ sec) indicating that the desorption stopped much more quickly. In all such cases, where the desorption rate was significant up to the maximum crystal temperature, some gas obviously remains in the crystal at the end of the desorption cycle. Subsequently heating the crystal to 2500°K for 30 sec caused some of this gas to desorb and had the important effect of making

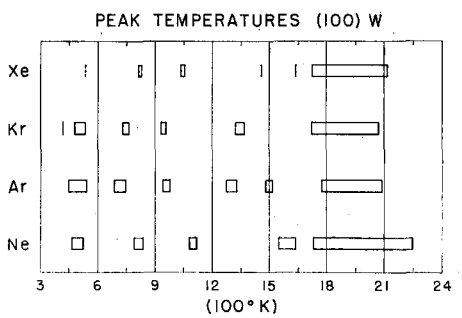

FIG. 8. Range of temperatures of all observed desorption peaks.

the desorption rate at 2400°K (and hence the influence on subsequent spectra) negligible.

Qualitatively similar results were obtained with argon, krypton, and xenon ions, as can be seen from the corresponding sets of spectra in Figs. 5, 6, and 7. In these three sets, the dose was 5×10^{12} ions/cm^2. For the heavier gases (Figs. 5–7) the peaks tended to be less clearly defined than for neon, and at least one additional α-peak could be seen. The α-peak amplitudes tended to become smaller with increasing ion mass, particularly at the highest energy. A careful examination of these spectra and others at intermediate energies has led to the identification of the peaks summarized in Fig. 8. The extent of the rectangles along the temperature axis indicates the range of temperatures over which the individual peaks have been observed to occur. The variations of the α-peak temperatures are due both to the interference between adjacent peaks (especially when their amplitudes differ greatly) and to uncertainties in the crystal temperature at the beginning of the desorption cycle. The latter arise from the very long times required to cool the crystal after heating; the average excess temperature after a desorption cycle being 40°K at 40 min, and 20°K at 1 h. The large variations of the β-peaks (Fig. 8) include their shifts upward with increasing ion energy. The lowest temperatures at which they appear are between 1700° and 1800°K for all four gases. Some similarity in the pattern of peak positions can be seen in Fig. 8, although variations with the type of ion are also apparent. The similarities are visible also in Fig. 9, which shows spectra for the four different ions at 600 eV. The amplitude scales in this case are not simply related; the β-peaks were arbitrarily made about equal in amplitude. The β-peak in Fig. 9 appears at the highest temperature in the Ne spectrum, lowest in the Xe spectrum.

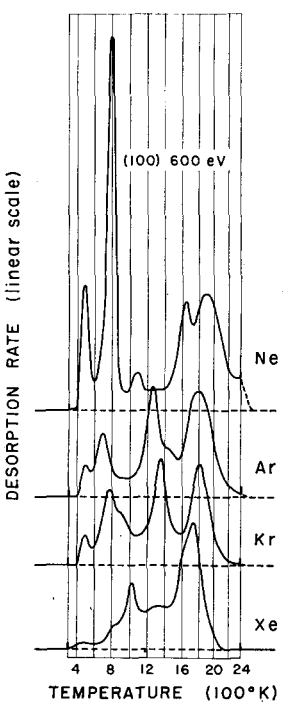

FIG. 9. Desorption spectra for 600 eV ions.

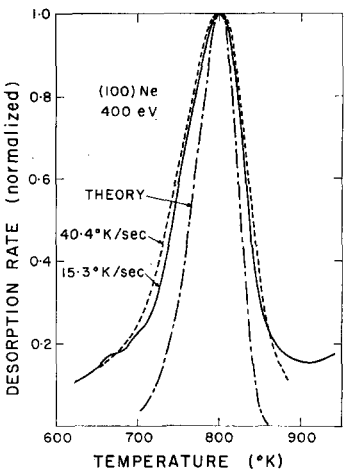

FIG. 10. Normalized profile of the 800°K peak in the neon spectra. The theoretical shape is derived from first-order desorption theory assuming a rate constant 10^{13} sec^{-1}.

A comparison of the 800°K peak of the neon spectra with theory is shown in Fig. 10. The theoretical curve is that expected for first-order desorption from sites of a single activation energy[1] using a rate constant 10^{13} sec^{-1}. Its width at half-amplitude is 62°K. The experimental curves show the expected asymmetry (steeper high-temperature side), but are 94° and 104°K wide for the two temperature rise rates 15.3°K/sec and 40.4°K/sec, respectively. The difference between the two experimental curves amounts to an increase of 0.25 sec in the width for the higher rise rate, probably attributable to the detection system time constant. The relatively broad "wings" on the experimental peaks below 0.2 indicate contributions either from nearby unresolved peaks or from sites distributed in activation energy. If we subtract a "continuum" of 0.15 from the 800°K peaks and renormalize, the remaining shapes agree very well with the theory. In any case, it is evident that the identified peaks alone (Fig. 8), if associated with discrete activation energies, cannot completely account for the observed desorption. Nevertheless the peak shapes suggest distinct, fairly well defined activation energies.

The effect of a 5 deg departure from normal ion incidence is shown in Fig. 11 for the case of 3 keV Ne^+. The high-temperature peak shifted from 2190° to 2040°K and its amplitude increased by 40%. The smaller changes in the low-temperature peaks are not considered significant. A change of similar magnitude was observed when the angle of incidence was made 45 deg [compare Fig. 4(b) with Fig. 7 of Ref. 13.]

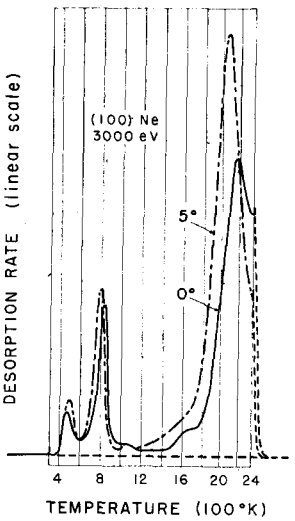

FIG. 11. Effect on 3000 eV Ne desorption spectrum of a 5 deg departure from normal incidence on a (100) surface.

Again the low temperature peaks were not significantly affected.

As described in I, the integration of the desorption spectra combined with a knowledge of the gauge sensitivity G (see Table I) and the system volume V allows the number of atoms desorbed, n_d, to be determined:

$$n_d = n_0 V \Delta P = (n_0 V/G) \int_0^t (di/dt)\, dt$$

where $n_0 = 3.27 \times 10^{19}$ molecules/Torr·liter at 300°K. Provided that the desorption cycle releases all the entrapped gas, the sticking probability of the ions, s, is given by the ratio of n_d to the total number of ions incident. When gas remains trapped in the target at the end of the desorption cycle (high ion energies), the above ratio gives an underestimate of the value of s. In Fig. 12 the sticking probability obtained as above is plotted against ion energy for the four gases incident normally on the (100) face. The absolute accuracy on the vertical scale is estimated to be $\pm 10\%$. The rapid increase of s at low ion energies is similar to that observed in I for polycrystalline tungsten. At high ion energies, the curves have been drawn dotted over the ranges where desorption of the gas was not complete and give lower bounds to s. In particular, the apparent decreases of s at the highest ion energies (Ne and Ar) are the results of incomplete desorption and are not physically realistic.

DISCUSSION

The primary result of these experiments, illustrated by Figs. 4–7, is that even for the simplest bombardment conditions (i.e., normal incidence of a small number of inert gas ions of a single energy on a clean, low-index crystal face) the desorption spectra indicate a complex array of binding energies of the trapped particles. As mentioned earlier, the desorption peaks can be divided into two qualitatively different types: all those below 1650°K being of one type (α-peaks), and the single peak above 1700°K of another type (β-peak). This division is the same as that made in I, where it was concluded that (a) the α-group of peaks were the result of single-step desorption from sites very close to the metal surface, and (b) the β desorption was associated with the diffusion of more deeply penetrating ions as impurities in the crystal. The evidence summarized below confirms these earlier conclusions, but on the basis of more clearly defined experimental conditions.

The α group of peaks have the following properties for all four ions: (1) The peak positions are independent of ion energy and of the direction of ion incidence (Figs. 4–7 and Fig. 7 of Ref. 13). (2) The peak shapes are reasonably consistent with first-order desorption from sites of a single activation energy (Fig. 10). (3) All the peaks can be seen at ion energies only twice the threshold value for entrapment.

We conclude from the above that most of the α-entrapment occurs in only four or five different kinds of sites. The differences might involve: (a) interstitial and substitutional positions in the lattice, (b) different distances from the site to the surface, (c) different locations of a nearby lattice defect (e.g., a vacancy) relative to the site and the surface.

The resulting variations in lattice relaxation could give rise to the series of characteristic binding energies observed. If a lattice defect is involved [(c) above] it must interact with the *particular* trapped atom that produced it, since the peaks exhibit first-order behavior. The appearance of all the α-peaks at ion energies so close to the threshold, and the independence of peak position on ion energy supports the

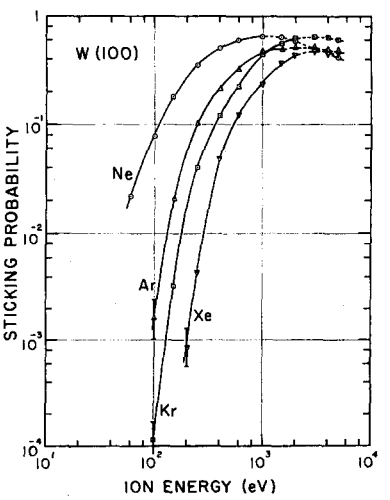

FIG. 12. The sticking probability of four ions at normal incidence as a function of ion energy. The dotted portions of the curves indicate that the gas desorption was incomplete and the calculated values of sticking probability too low.

earlier conclusion that the sites must be very close to the crystal surface and must involve desorption via a single activation step. The fact that the different gases give roughly similar peak patterns (Figs. 8 and 9) suggests that they occupy, to a first order, the same kinds of sites. The minor changes in the number of peaks and their positions would imply that there are some configurations which are stable for some ions but not for others, and that for a given site the lattice relaxation and therefore the binding energy varies somewhat with the particular ion trapped. This is in contradiction to the conclusion drawn in I that the binding energies were not dependent on which ion was trapped. The more clearly defined spectra and more reliable desorption and detection system have allowed us to see differences and variations which could have been missed in the earlier work. It should be noted that the spectra presented here are in a general way similar to those in I for the same bombarding conditions.

Since the maximum probability of entrapment in an "α-site" is about 0.4 (Ne^+ at 600 eV), it seems likely that the sites involve configurations related to the perfect crystal lattice rather than to anomalies such as previously existing point defects or atomic steps. An estimate of the depth over which the α-sites extend can be obtained by comparison of the present data with those on ion penetration depth. For 400 eV Xe^+ ions, it was found (Kornelsen *et al.*[17]) that 99% of the trapped gas was removed upon the removal of a layer of tungsten $10(\pm 2)$ Å thick. This means that the trapped gas was confined to a layer of this thickness and strongly suggests that the maximum penetration depth cannot have been greater. The spectrum for 400 eV Xe^+ (Fig. 7) contains all five peaks of the α-group, allowing the conclusion that the xenon α-sites are all within at most 10 Å (three lattice constants) of the surface. A similar argument, using unpublished penetration data, can be shown to give the same result for krypton ions. In view of the similarities of the peak patterns for the different gases (Figs. 8 and 9), it seems reasonable to assume the same depth to apply to all the α-sites.

The decreasing amplitude of the α-peaks with increasing energy [Fig. 4(b)] was subsequently found to be an interaction effect between the trapped atoms and later arriving ions. At a dose of 3×10^{11} ions/cm^2, the amplitudes increased with energy up to $\sim$1 keV and were almost constant above 1 keV. At higher doses, later arriving ions induce the desorption of those trapped earlier in the bombardment, the desorption efficiency increasing with increasing energy. The gas trapped in α-sites is extremely sensitive to surface disturbance, the area affected by a single ion exceeding 10^{-13} cm^2 above 1 keV. More detailed numerical results are presented in Ref. 13. The mechanism described above is undoubtedly responsible for the similar amplitude decreases observed in I.

The β desorption peak has the following properties:

(1) It is present only for ion energies $\geq$400 eV, but dominates the spectra above 2 keV.

(2) The lowest temperature at which it appears (i.e., at the lowest ion energy) is between 1700° and 1800°K for all four gases (Fig. 8).

(3) Its position shifts monotonically to higher temperature with increasing ion energy; the largest shifts being $>$300°K (Fig. 8).

(4) It has a width at half amplitude of $\sim$500°K and, unlike the low temperature peaks (Fig. 10), is approximately symmetrical.

(5) For high ion energies ($>$1 keV) its position is sensitive to the direction of ion incidence (Fig. 11) (see also Ref. 13).

The above observations are consistent with a desorption occurring via the diffusive motion of inert gas within the crystal. In line with the conclusion drawn above for the α-sites, we suggest that these are ions which have penetrated more than about 10 Å into the crystal and that the influence of the surface on their activation energy of motion is negligible so that they diffuse as bulk impurities. The peak temperature variation with energy and direction of incidence is caused by the time required for the atoms to diffuse from varying depths within the crystal. The rapid variation of peak position with incident angle (Fig. 11) is attributable to channeling which causes a large increase in penetration when the ions are directed very close to the $\langle 100\rangle$ axis in the crystal.

An estimate of the variation of peak temperature with penetration depth can be obtained from a modification of the first-order desorption equation

$$d\sigma/dt = -\sigma\gamma_1 \exp(-E/RT), \qquad (1)$$

where σ is the number trapped, γ_1 the first-order rate constant, and E the activation energy of desorption. This equation has been solved for a linear temperature rise rate $T=T_0+\beta t$,[1] yielding the peak temperature T_p as a function of E for a series of values of the ratio γ_1/β. For an atom executing a random-walk motion, as in isotropic diffusion, Eq. (1) describes the atomic "stepping" rate ds/dt rather than the desorption rate. If the atoms make, on the average, N steps before desorption, then the desorption rate would be

$$d\sigma/dt = (1/N)(ds/dt) = -(\sigma\gamma_1/N)\exp[-E/RT], \qquad (2)$$

where E is now the activation energy of diffusion. Random-walk theory suggests (see, for example, Ref. 18) that for an atom a linear distance n steps from a surface, $N\approx n^2$. Thus the solutions[1] to the desorption equation (1) are applicable with γ_1/β replaced by $\gamma_1/\beta n^2$. An identical conclusion has been drawn

[18] P. G. Shewmon, *Diffusion in Solids* (McGraw-Hill Book Co., New York, 1963).

TABLE II. Temperature width of β peaks.

	Kr		Xe	
Bombarding energy	5 keV		5 keV	
Median range R_m[a]	53		37	
Peak temperature T_p (°K)	2080		2180	
Measured width $(\Delta T)_{1/2}$ (°K)	530		510	
Calculated widths at half-height (°K)[19]	$\nu_1=10^{13}$	$\nu_1=10^{15}$	$\nu_1=10^{13}$	$\nu_1=10^{15}$
(a) Plane source (all atoms at depth R_m)	272	241	281	248
(b) xe^{-x} distribution	393	353	405	364
(c) e^{-x} distribution	500	450	515	465

[a] 10 Å has been subtracted from the measured median penetrations[17] and the remainder expressed in units of the ⟨100⟩ interplanar spacing.

by Erents and Carter[3] on the basis of the diffusion equations.

To apply the above result to the present data, we first assume that E can be obtained from the minimum temperature $(T_p)_{\min}$ at which the β-peak appears, i.e., that for this case $n=1$. Experimentally $(T_p)_{\min}$ has an average value for the four gases of 1720°K (Fig. 8). For $\beta=40$°K/sec, assuming $\gamma_1=10^{13}$ sec^{-1}, we obtain $E=104$ kcal/mole (4.50 eV). To a first approximation, let n be the median penetration, R_m, minus the 10 Å depth occupied by the α-sites. For 5 keV Xe^+ ions, $R_m=13$ μg/cm^2=67.5 Å[17] or, in units of the ⟨100⟩ interplanar distance of 1.58 Å, $n=37$. Again using $\gamma_1=10$,[13] the predicted value of T is 2210°K (a 490°K shift), whereas the measured value (Fig. 7) is 2180°K (a 460°K shift). The peak shift is thus consistent with isotropic diffusion of trapped atoms with a single activation energy, which can be obtained from the minimum value of T_p using Eq. (1).

Approximate expressions for the width of the desorption peak, including the effect of initial depth distribution, have been derived.[19] A comparison of the predictions with the experimental values for two clearly defined cases is given in Table II. The calculations for a "plane" distribution are for all the atoms initially at a depth equal to the median range R_m. Kelly *et al.*[19] suggest that the rate constant γ_1 should be $10^{15\pm1}$ sec^{-1}, whereas sweep rate variations[5] have suggested a value $10^{13\pm1}$ sec^{-1} for polycrystalline tungsten. Both values of the rate constant have been included to indicate the sensitivity to this parameter. The depth distributions have been found experimentally to be fairly close to the exponential form e^{-x} for 5 keV ions.[17] The agreement between calculated and experimental peak widths for the exponential distribution case (Table II) is seen to be fairly good, again suggesting isotropic diffusion with a single activation energy, and a rate constant near 10^{13} sec^{-1}.

The sticking probability curves (Fig. 12) have qualitatively the same shape, below 2 keV, as those in I. The ion energies for a given sticking probability s, however, are approximately 0.7 of those found in I, a decrease attributable, at least in part, to the fact that all the ions in the present experiments are incident normally on the surface.

The conclusion was drawn in I, based on calculations of the interatomic potential energy,[20,21] that the threshold energy for entrapment was associated with the conversion of most of the kinetic energy of the ion to potential energy in the first one or two atomic planes of the crystal. The present results support this conclusion, the lower threshold energies simply suggesting a slightly greater relaxation of the lattice during the impact.

A simple extension of the arguments mentioned above has been used[22] to calculate the sticking probability of He, Ne, Ar and Kr ions incident normally on a (100) tungsten surface with energies up to 1 keV. In general, their calculated values agree well with Fig. 12 even though their initial assumptions (namely, that hard sphere collisions are involved, that every collision leads to reflection, and that relaxation of the lattice atoms during the collision is negligible) are not very realistic.[23] The good agreement suggests that the combined effect of choosing a more realistic collision model and a more accurate interatomic potential, and taking lattice relaxation into account will not be large.

The tendency to a value of s less than one, and varying slowly with ion energy above 1 keV, is again very similar to I. The apparent decrease of s due to incomplete desorption is considerably larger than in I, a direct result of the large penetration depth of the ions along the ⟨100⟩ channel.

CONCLUSIONS

The following main conclusions can be drawn from the results presented in this paper:

(1) Desorption spectra have been obtained which are characteristic of the entrapment of very small numbers of inert gas ions on a flat, clean (100) tungsten face.

[19] R. Kelly, C. Jech, and H. J. Matzke, Phys. Status Solidi **25**, 641 (1968).

[20] A. A. Abrahamson, Phys. Rev. **130**, 693 (1963).

[21] A. A. Abrahamson, Phys. Rev. **133**, 990 (1964).

[22] K. J. Close and J. Yarwood, Brit. J. Appl. Phys. **18**, 1593 (1967).

[23] In particular it should be pointed out that at the threshold energy an inconsistency of a factor two arises from these assumptions: The penetrating ions in this case interact simultaneously with two equidistant lattice atoms, whereas their calculation in effect considers only one.

(2) Even for these simplest attainable bombarding conditions, at least as many as five (Ne) or six (Ar, Kr, Xe) characteristic energies of binding exist.

(3) All desorption peaks below 1650°K are associated with entrapment of the ions within at most 10 Å of the crystal surface. The binding energies are probably determined by specific arrangements of the neighboring lattice atoms (and possibly vacancies) around the trapping, site, with the resulting lattice relaxation being strongly influenced by the proximity of the surface.

(4) The single peak appearing above 1700°K is associated with the isotropic diffusion of gas atoms which have been trapped at distances >10 Å from the surface. The variation of position and width of the peak with penetration depth, and the lowest temperature at which it appears are all consistent with a single activation energy of diffusion of 104 kcal/mole (4.50 eV/atom) applicable to all the gases, and with a first-order rate constant within one order of magnitude of 10^{13} sec^{-1}.

(5) The sticking probabilities at low ion energies suggest that the threshold for entrapment is determined by the potential energy barrier encountered by the ions in passing through the first one or two atomic planes at the crystal surface.

ACKNOWLEDGMENTS

The authors are pleased to acknowledge many fruitful discussions with their colleagues P. A. Redhead, J. P. Hobson, and R. A. Armstrong. We are indebted to the technical staff of the Electron Physics Section, particularly to A. W. Pye, R. D. Cottee, and J. O. Weeks, who built the vacuum system, and R. Chapman who developed the electronic circuits.

JOURNAL OF APPLIED PHYSICS VOLUME 39, NUMBER 10 SEPTEMBER 1968

Computed Shock Response of Porous Aluminum

RONALD HOFMANN, DUDLEY J. ANDREWS, AND D. E. MAXWELL
Physics International Company, San Leandro, California 94577

(Received 30 October 1967; in final form 22 February 1968)

The shock response of powdered aluminum compacted by a driver plate was simulated with a one-dimensional Lagrangian continuum mechanics computer program. The porous aluminum was mocked up by a series of flat plates separated by gaps to obtain an initial density of 1.35 g/cm³ for the "powder." The compaction process was followed in detail for two cases of driver-plate conditions corresponding to two Stanford Research Institute experiments. The calculations showed an approach to equilibrium behind the shock in each of the porous samples. The equilibrium states established were found to be consistent with the Rankine–Hugoniot jump conditions applied to aluminum of density 1.35 g/cm³. These states did not lie on the Hugoniot curve of solid-density aluminum. This was shown to be due to the significant internal-energy dependency in the equation of state. The calculated results were in good agreement with the SRI experiments. Application of this computational model to more complex cases is indicated.

I. INTRODUCTION

Two conflicting views exist regarding the equilibrium states reached when a porous metal is compacted by a shock of a few hundreds of kilobars: the view of Thouvenin[1] and the conventional view.

Thouvenin has presented the view that the interacting particles of a porous metal result in an equilibrium state situated on the Hugoniot curve of the solid metal. He reached this conclusion as a result of hand calculations applied to the (one-dimensional) porous material mock-up shown in Fig. 1. He traced the primary signal paths and followed typical particle histories in the approach to equilibrium. His analysis depended upon the key simplifying assumption that the pressure in the porous metal depended almost entirely on compression, i.e., internal-energy dependency was negligible. This assumption is consistent with Hugoniot data obtained from shock experiments on solid metals in the pressure range in question but, unfortunately, this type of experiment produces data that are insensitive to internal-energy dependency. In fact, this limitation has been one of the motivations for performing shock experiments on porous metals.

In the view juxtaposed to Thouvenin's, the only assumption made is that an equilibrium state is approached behind the shock front and that this state and the shock velocity are consistent with the Rankine–Hugoniot jump conditions. The jump conditions themselves are firmly grounded in conservation principles and must apply if an initial uniform steady state is transformed to a final uniform steady state at a constant rate; therefore, if a finite transition region exists, it must have a constant mass and thick-

[1] J. Thouvenin, *Proceedings, Fourth Symposium (International) on Detonation* (U.S. Naval Ordnance Laboratory, Silver Springs, Md., Oct. 1965), Vol. 1.